Multiphase Science and Technology, Vol. 21, No. 1–2, pp. 81–93, 2009

VOLUME FLOW RATE MEASUREMENT IN VERTICAL OIL-IN-WATER PIPE FLOW USING ELECTRICAL IMPEDANCE TOMOGRAPHY AND A LOCAL PROBE

Hua Li,[1] Mi Wang,[1] Ying-Xiang Wu,[2] and Gary Lucas[3]

[1]*Institute of Particle Science and Engineering, University of Leeds, Leeds LS2 9JT, United Kingdom*

prehli@leeds.ac.uk, m.wang@leeds.ac.uk

[2]*Institute of Mechanics, Chinese Academy of Sciences, Beijing 100080, China*

yxwu@imech.ac.cn

[3]*School of Computing and Engineering, University of Huddersfield, Huddersfield HD1 3DH, United Kingdom*

Abstract. This paper presents the use of a high-performance dual-plane electrical impedance tomography (EIT) system and a local dual-sensor conductance probe to measure the vertical upward cocurrent oil-in-water pipe flows. Experiments were carried on a flow loop with a transparent 2.5-m-long, 80-mm inner diameter test section using kerosene and tap water. The flow conditions were predominantly of the dispersed type, with nonslip oil volume fractions of 9.1, 16.7, and 23.1%, respectively, and with two groups of different mixture velocities. A sensitivity coefficient back-projection algorithm was adopted to reconstruct the flow distributions from the EIT measurement data, and then the oil in situ volume fraction was calculated based on a Maxwell relationship with temperature compensation. The oil velocity distribution was obtained using a pixel-to-pixel cross-correlation method. A local intrusive conductance probe was adopted to supply a reference measurement of oil volume fraction and velocity profiles. The oil volume fraction and velocity distributions from the two techniques were compared and good agreement was found. A further calculation of the water velocity distributions and flow rates was implemented through the drift flux approach and the results were analyzed and discussed.

1. INTRODUCTION

Two-phase flow of oil and water is commonly observed in the petroleum industry, where they are produced and transported together. For example, oil water flow in wellbore is often encountered when oil fields mature and the coproduction of water generally increases with time. However, such flows have not been studied to the same extent as gas–liquid flows.

In petroleum engineering applications, the flow pattern, holdup, and velocity of the two phases are very important hydrodynamic features. The complexity of two-phase flows lies in the various configurations of interface distribution and nonuniform velocity profiles, and it constitutes a still unresolved issue for the petroleum industry.

Process tomography is an emerging measurement technology with applications in a broad range of industries. It is unintrusive and provides a means of obtaining detailed local flow information such as phase and velocity distributions, which can help us to understand flow processes better and is beneficial in process monitoring and control. Due to its capability of obtaining local detailed flow distribution, it is promising to overcome the main challenge of multiphase flow measurement. However, only a few investigations could be found in oil–water flow and even less with the electrical tomography.

In two-phase flow metering, it is usually hard to obtain all parameters of both phases. Thus, modeling techniques are also required to predict and interpret the results. In this study, a drift-flux approach was adopted to analyze the velocity slippage phenomenon. The drift-flux model proposed by Zuber and Findlay (1965) is widely used to represent two- and three-phase flow in pipes and wellbores. It has been refined by Flores *et al.* (1998) and Hasan and Kabir (1999) for modeling oil–water flow in vertical and deviated wellbores, and their investigation also showed significant slippage occurred in water-dominated flow patterns.

The objective of this work is to investigate and validate the application of electrical impedance tomography (EIT) system for metering such flows as oil-in-water vertical pipe flow in which the continuous component is electrical conductive. The local volume fraction distributions obtained using EIT can be erroneous to a certain level, because they are highly sensitive to such factors as the accuracy of the electrical measurements made at the system boundary and the image reconstruction algorithm that is used (Dickin *et al.*, 1993). At a measurement error of 1%, the conductivity error could rise to 10%, subjective to the magnitude of conductivity charge (Wang *et al.*, 1999). Given these facts, it is important to conduct reference measurements with an independent technique. A local intrusive dual-sensor conductance probe was employed for this purpose in this study.

2. EXPERIMENTAL SETUP AND DATA PROCESSING

2.1 *The flow loop*

The experiments were carried in a flow loop built at University of Huddersfield with a 2.5-m long, 80-mm internal diameter, transparent, vertical working section, which is

shown in Fig. 1. Water and oil were respectively pumped into the base of the working section via different branches with turbine meters which enabled the water volumetric flow rate Q_w and the oil volumetric flow rate Q_o to be measured.

Two groups of tests were carried out with water flow rates at 5 and 7.5 m^3/h, and oil flow rates at 0.5/1/1.5 and 0.75/1.5/2.25 m^3/h, respectively, which allowed predominantly dispersed type flow conditions, with nonslip oil volume fractions of 9.1, 16.7, and 23.1%, respectively, and with two groups of different mixture velocities.

2.2 *The EIT system and data processing*

Leeds University has developed a new EIT system for online measurement of two-phase flows which is capable of metering axial velocity of 10 m/s with 5% velocity measurement resolution (Wang *et al.*, 2005). The distance between the dual planes of

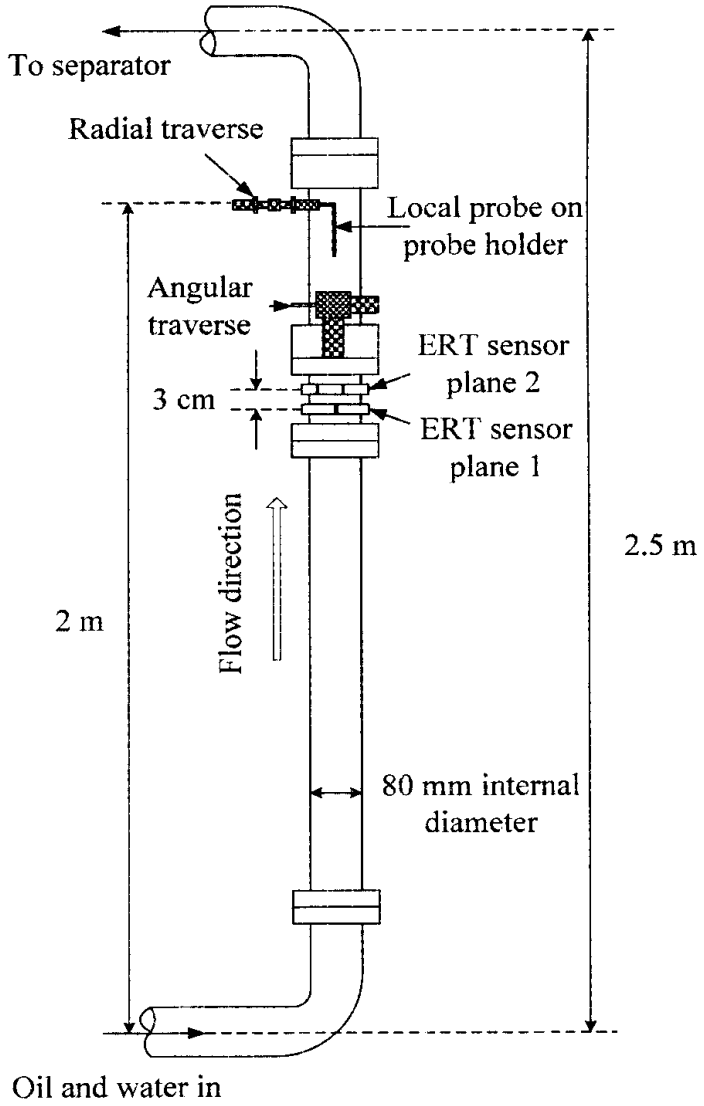

Figure 1 Schematic of the test section.

the EIT sensor with 16 electrodes per sensing plane was 30 mm. A total of 8190 dual-frames of voltage measurements were acquired for each flow condition, which took 8.96 s at a speed of 914.3 dual-frames per sec (dfps). A sensitivity coefficient back-projection (SBP) algorithm was adopted to reconstruct flow images for its high speed, which adopted 316 square meshes.

2.2.1 *Concentration calculation*

With conductivity distributions from EIT, the oil concentration distributions (expressed as oil volume fraction, α_o) can be determined by applying the Maxwell relationship (Maxwell, 1881),

$$\alpha_o = \frac{2\sigma_w - 2\sigma_m}{2\sigma_w + \sigma_m} \tag{1}$$

where σ_w is the conductivity of water and σ_m is the local mixture conductivity. This is a simplified form in consideration of the conductivity of oil being zero.

The reconstruction algorithm uses the voltage relative changes between a measurement profile acquired from a flow with concentration change and a reference profile acquired from a flow with water only. Since the water temperature, and therefore, the conductivity, usually arises during the experimental process, a reference profile has to be compensated based on the water temperature. The relationship between voltage and temperature can be approximated as (Wang *et al.*, 2003)

$$V_{T_2} = V_{T_1} e^{-0.0243(T_2 - T_1)} \tag{2}$$

which is an empirical relation based on tests where V_{T1} and V_{T2} are the voltages responding to a linear system at temperatures T_1 and T_2, respectively.

2.2.2 *Velocity calculation*

The axial flow velocity distributions can be estimated by a direct cross-correlation method, as given in Eq. (3),

$$R_{12}^{(k)}(n) = \sum_{m=1}^{k} f_1(m) f_2(m+n) \tag{3}$$

where k is the sample length, n is the offset number, and $f_1(m)$ and $f_2(m)$ are the mth upflow and downflow images, respectively. Equation (3) can be simply implemented online by updating the $R_{12}^{k}(n)$ with the new (k+1) images, as described in the following:

$$R_{12}^{(k+1)}(n) = R_{12}^{(k)}(n) + f_1(k+1) f_2(k+1+n) \tag{4}$$

This implementation can save calculation time and reduce memory size greatly (Wang *et al.*, 2005).

2.2.3 *Volumetric flow rate calculation*

The phase volumetric flow rate Q_i can be obtained by integrating the product of the local volume fraction α_i and axial velocity v_i of the specified phase in the flow cross section according to the equation $Q_i = \int_A \alpha_i v_i dA$, where A denotes the cross section area.

2.3 *The local dual-sensor conductance probe*

The dual-sensor probe was constructed at University of Huddersfield. Each probe was manufactured from two stainless steel acupuncture needles which were 0.3 mm in diameter and were mounted inside a stainless steel tube with an outer diameter of 4 mm, as shown in Fig. 2 (Lucas *et al.*, 2004). Each acupuncture needle was coated with waterproof paint and insulating varnish, except the very tip of the needle. The two needle tips of the probe are separated by an axial distance s of 5 mm and a lateral distance of 1 mm.

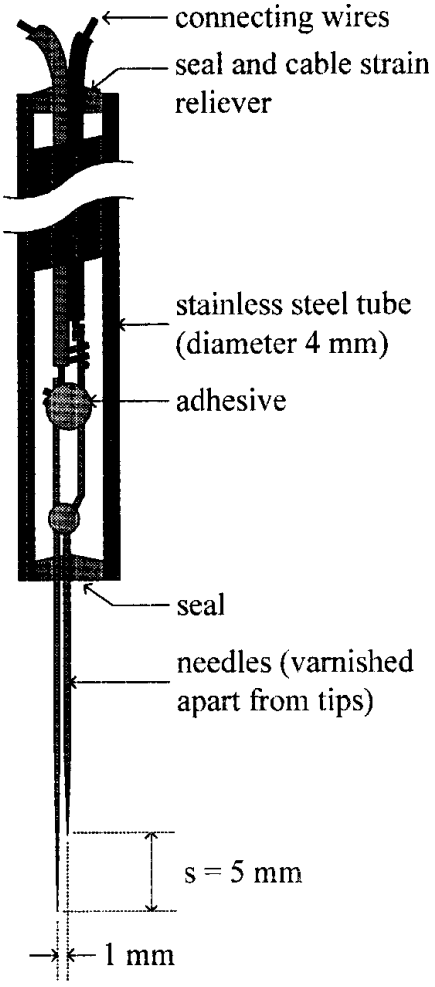

Figure 2 Construction of the probe.

2.3.1 *The traversing mechanism*

The dual-sensor conductance probe was mounted in a fully automated, two-axis traversing mechanism which enabled the probe to be moved to different spatial location in the measurement plane. In the experiments, the probe was traversed following two sets of parameters. One is across four equiangled diameters with 15 equispaced locations on each diameter, giving a total of 57 distinct measurement locations, respectively; the other is 8 equiangled diameters with 11 equispaced locations on each diameter, giving a total of 81 distinct measurement locations. At each measurement location, data were acquired from the dual-sensor probe for a period of 30 s for one test.

2.3.2 *The operational principle*

The principle of operation can be briefly explained as follows (Lucas *et al.*, 2004). Consider an idealized situation in a vertical upward oil–water bubble flow in which the bubbles are assumed to travel in the axial direction only. When the surface of an oil bubble makes first contact with the upstream (front) sensor at time t_{1f}, the measured conductance at the front sensor will fall sharply (see Fig. 3) as it is immersed in oil instead of water. Then when the front sensor makes last contact with the surface of the bubble at time t_{2f} (i.e., the time at which the bubble leaves the front sensor), the measured conductance at the front sensor will rise sharply as the sensor is immersed in water again. The corresponding times of the rear sensor are t_{1r} and t_{2r}, respectively.

Assume N bubbles hit both the front and rear sensors during a sampling period T. For the ith bubble, two time intervals could be defined as follows:

$$\delta t_{1,i} = t_{1f,i} - t_{1r,i} \tag{5}$$

$$\delta t_{2,i} = t_{2f,i} - t_{2r,i} \tag{6}$$

The mean local oil bubble velocity u_{ol} at the measurement position is then given by

$$u_{ol} = \frac{2s}{N} \sum_{i=1}^{N} \frac{1}{\delta t_{1,i} + \delta t_{2,i}} \tag{7}$$

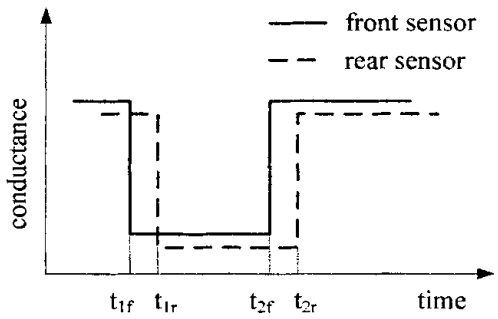

Figure 3 Ideal signals when an oil bubble strikes the probe.

The mean local oil volume fraction α_{ol} can be estimated from the conductance signal from either the front or the rear sensor (Serizawa *et al.*, 1975). For the front sensor, α_{ol} is given by

$$\alpha_{ol} = \frac{1}{T}\sum_{i=1}^{N}(t_{2f,i} - t_{1f,i}) \tag{8}$$

The oil volume flow rate calculation is similar with that of EIT, except here the summation is over concentric annuli and in the EIT situation it is over square pixels.

2.4 *Drift flux model*

The basic form of the drift flux model in oil–water flow is

$$V_o = C_o V_m + V_d' \tag{9}$$

where V_o is the velocity of the oil phase, C_o is the distribution parameter, V_m is the mixture velocity, and V_d' is the oil drift velocity.

Based on Hasan and Kabir's (1999) work, the oil drift velocity is given by

$$V_d' = 1.53 v_c'(1 - \alpha_o)^2 \tag{10}$$

where v_c' is the characteristic velocity; it was deduced by Harmathy (1960) in gas–liquid flows. The corresponding form in oil–water flow could be expressed as

$$v_c' = \left[\frac{\sigma_{ow} g(\rho_w - \rho_o)}{\rho_w^2}\right]^{1/4} \tag{11}$$

where σ_{ow} is oil–water surface tension, g is gravitational acceleration, and ρ_w and ρ_o are densities of water and oil, respectively.

In this paper, the volume fraction and velocity distributions of oil were already obtained. The purpose of adopting the drift-flux model was to calculate the relative velocity between oil and water, which is given by

$$v_r = \frac{V_d'}{1 - \alpha_o} \tag{12}$$

The drift-flux model is originally a one-dimensional model, but here, based on the assumption of the influence of oil concentration on oil drift velocity mainly happening in the axial direction, the relative velocity was calculated pixel by pixel. Then further calculation of water velocity distribution and volume flow rate could be conducted.

3. RESULTS AND DISCUSSIONS

According to Beck and Plaskowski (1987), the minimum acquisition time δ can be taken as twice the product of the minimum transit time of the fluid τ, and the fractional velocity discrimination κ is given in the following

$$\kappa = \frac{\delta}{2\tau} \tag{13}$$

The discrimination resolution of the EIT system calculated from Eq. (13) in this study is about 1%, which is a big advance compared with previous work (Wu *et al.*, 2005). The potential of the EIT system to obtain local flow distributions can be shown in Fig. 4.

3.1 *Comparison of oil concentration and velocity profiles*

To compare with the results of the probe, the cross-sectional distributions of EIT were averaged along the radial axis and are shown together with probe results in Figs. 5 and 6. SBP denotes the results of EIT adopting the SBP reconstruction algorithm, 4d15p denotes results of the probe averaged from 4 equiangled diameters with 15 equispaced measurement points on each diameter, and 8d11p denotes results of the probe averaged from 8 equiangled diameters with 11 equispaced measurement points on each diameter.

Good agreement was found in both oil concentration and velocity profiles. Due to the intrusiveness of the probe, the oil bubbles were slowed down, which caused a decrease in velocity and an increase in concentration. The wall peak phenomenon is evident in the profiles from both techniques, but the intrusive essence of the probe is accompanied by the simplicity of operational principle, which gives a more precise profile form.

The underestimation of concentration from EIT could also be caused by the temperature difference between the EIT sensor position and the temperature measurement position, which is located in the water storage tank where the temperature is a little lower.

The SBP algorithm results in flat concentration profiles, but this is not the case in the velocity profiles. There is a sudden drop near the center and a flat distribution near the wall. The latter could be caused by the system noise, but the former could be related to both the hardware and the reconstruction algorithm.

Finally, the difference is also due to the unsteady flow status. The EIT and probe were operated in different times based on the same water and oil flow rates as read by turbine flow meters. For one flow condition, EIT needs only about 9 s but the probe needs at least 30 min, so EIT results are more easily affected. The measurement location

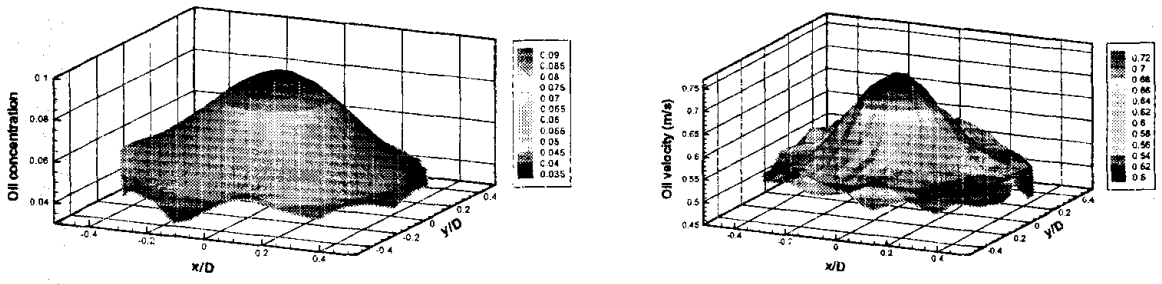

Figure 4 Oil concentration and velocity distributions from EIT (Q_w = 7.5 m^3/h, Q_o = 0.75 m^3/h).

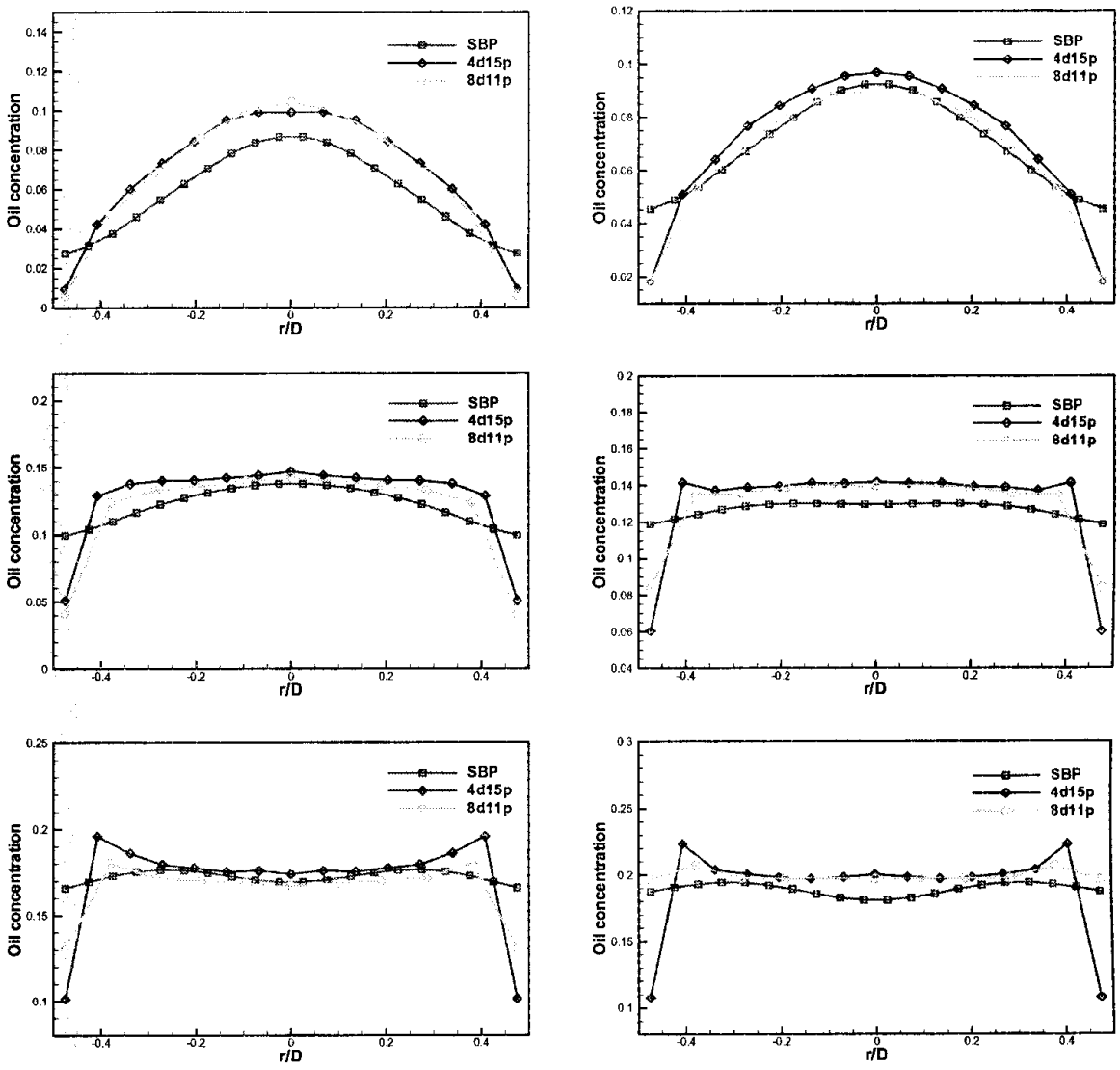

(a) Q_w=5 m^3/h, Q_o=0.5/1/1.5 m^3/h (b) Q_w=7.5 m^3/h, Q_o=0.75/1.5/2.25 m^3/h

Figure 5 Oil concentration profiles from EIT and the probe.

of the probe is a little higher than EIT, which is around 25 and 20 times the inner diameter of the pipe. In this range, the flow is also developing and there is a slight difference.

3.2 *Oil and water flow rates*

Oil flow rates can be calculated based on the concentration and velocity profiles. Furthermore, with the drift-flux model, the water velocity distributions and then flow rates can also be calculated. The results are shown in Fig. 7, where the left side of Fig. 7(b) shows the results under different oil flow rates while the water flow rate is fixed at 5 m^3/h, and the right side shows the results when the water flow rate is fixed at 7.5 m^3/h.

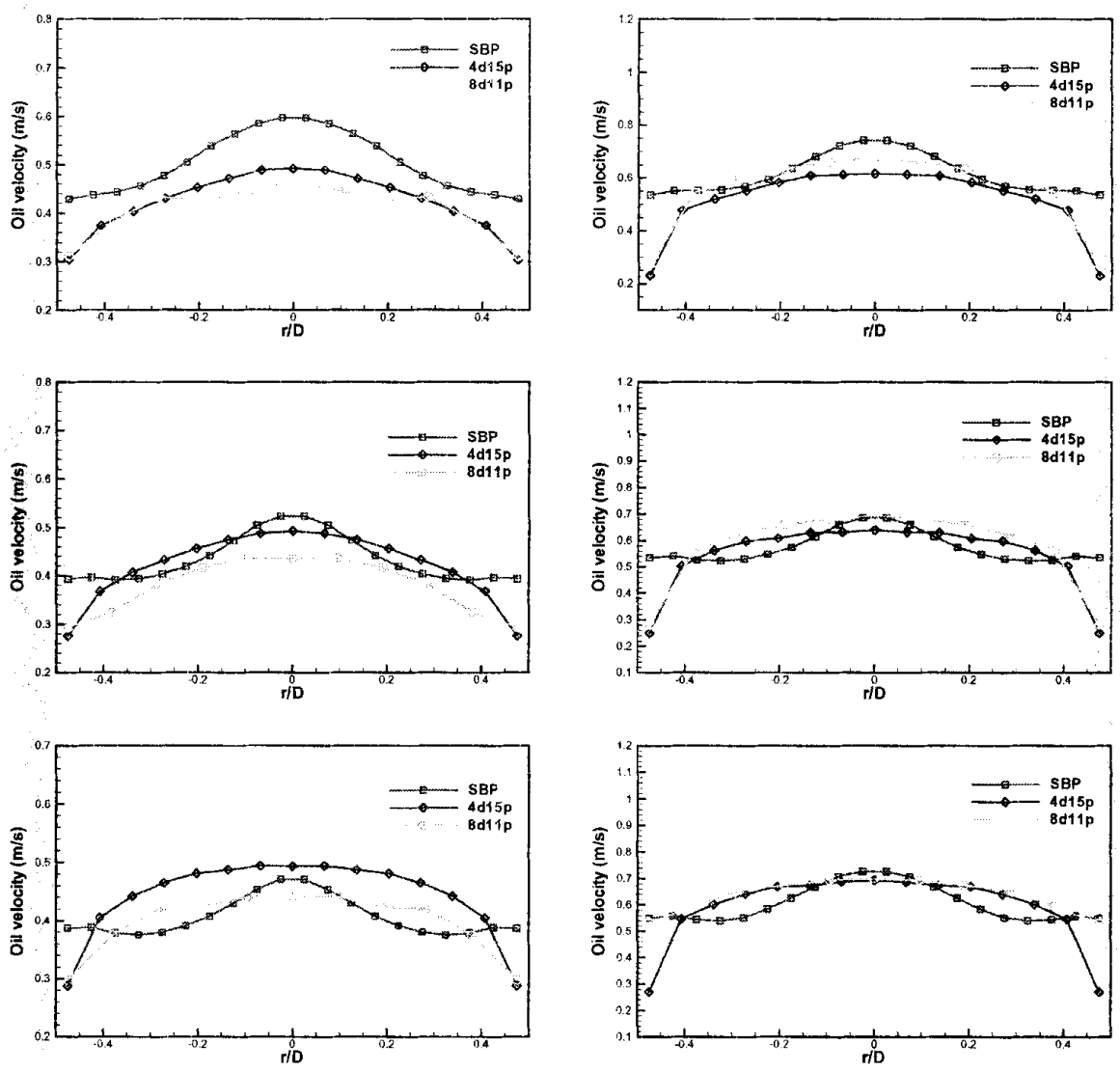

(a) Q_w=5 m^3/h, Q_o=0.5/1/1.5 m^3/h (b) Q_w=7.5 m^3/h, Q_o=0.75/1.5/2.25 m^3/h

Figure 6 Oil velocity profiles from EIT and the probe.

For the oil flow rates, better results are obtained from the probe, mostly within an error range of 10%. The EIT results have an obvious underestimation, and all results are between the error range of −10 and −20%. As stated above, this is caused by the underestimation of the concentration and the imprecise form of the velocity profile.

For the water flow rates, the nonslip model has a significant overestimation, and with the drift-flux model, most results are close to the error range of 10%, which shows that a significant slippage exists in the flow. Since the flow is still developing, the drift-flux model has a slight overestimation of the relative velocity, which sequentially causes lower water flow rates.

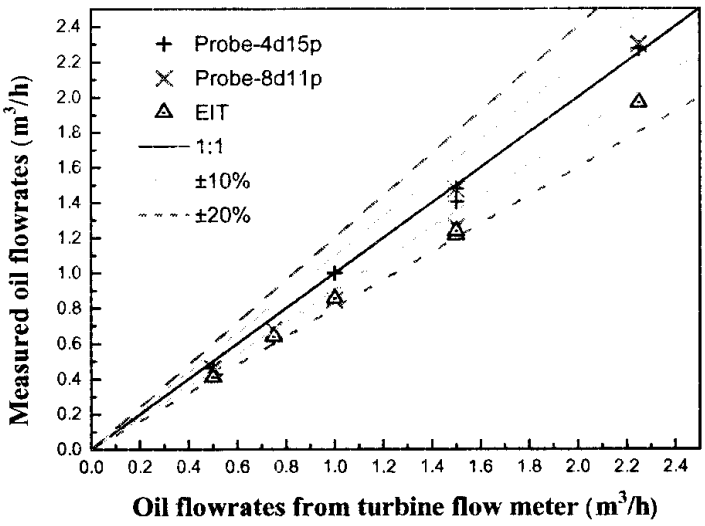

(a) Oil volume flowrates from EIT and probe

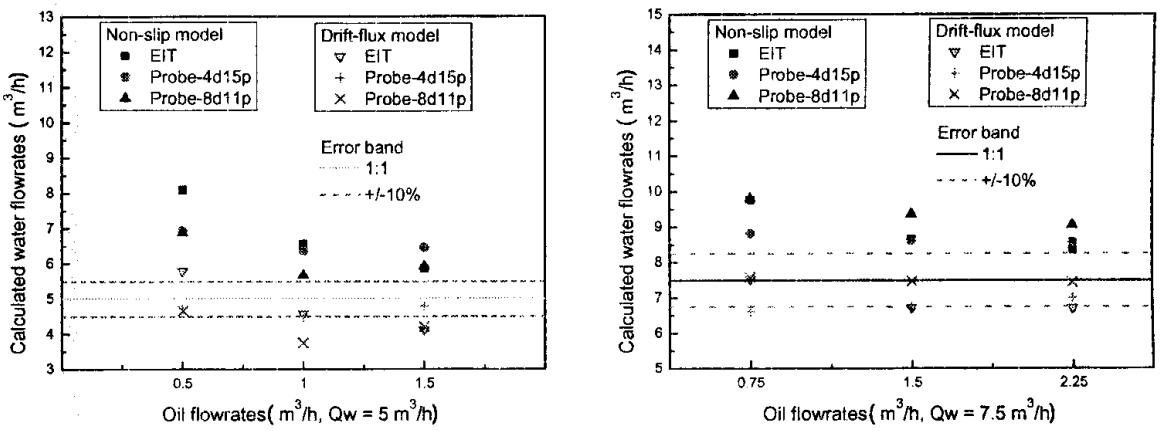

(b) Water volume flowrates from EIT and probe

Figure 7 Comparison of oil and water volume flow rates.

4. CONCLUSIONS

A study of vertical oil-in-water flow has been conducted to measure the concentration and velocity profiles and then flow rates of both phases. The following conclusions from this study are listed below:

- Good agreement was found in the oil volume fraction and velocity profiles between EIT and the probe.
- Due to the difference in operational principle and unsteady flow conditions, probe results provide a better description of the profile form.
- The accuracy of concentration calculation with EIT relies significantly on the conductivity of water, which caused an underestimation of the oil concentration.

- Significant slippage was found in the oil-in-water flow, and the drift-flux model is an effective approach to describe it.
- A reconstruction algorithm for EIT with improved precision and proper speed is needed to obtain more accurate results in on-line measurement.
- EIT is an unintrusive technique with the capability to obtain detailed flow information. It is a promising approach for two-phase flow measurement with appropriate modeling and calibration.

ACKNOWLEDGMENT

The authors acknowledge Marie Curie Actions (EU FP6) for supporting this work.

REFERENCES

Beck, M. S. and A. Plaskowski (1987), Cross Correlation Flowmeters: Their Design and Application, Bristol: Adam Hilger.

Dickin, F. J., Williams, R. A., and Beck, M. S. (1993), Determination of Composition and Motion of Multicomponent Mixtures in Process Vessels using Electrical Impedance Tomography —I. Principles and Process Engineering Applications, *Chem. Eng. Sci.*, **48**, 1883.

Flores, J. G., Sarica, C., Chen, T. X., and Brill, J. P. (1998), Investigation of Holdup and Pressure Drop Behavior for Oil–Water Flow in Vertical and Deviated Wells, *JERT, Trans. ASME*, **120**, 8.

Harmathy, T. Z. (1960), Velocity of Large Drops and Bubbles in Media of Infinite and Restricted Extent, *AICHE J.*, **6**, 281.

Hasan, A. R. and Kabir, C. S. (1999), A Simplified Model for Oil/Water Flow in Vertical and Deviated Wellbores, *SPE Prod. & Fac.*, **14**, 56.

Lucas, G. P., Mishra, R., and Panayotopoulos, N. (2004), Power Law Approximations to Gas Volume Fraction and Velocity Profiles in Low Void Fraction Vertical Gas–Liquid Flows, *Flow Meas. Instrum.*, **15**, 271.

Maxwell, J. C. (1881), A Treatise on Electricity and Magnetism, Oxford: Clarendon Press.

Serizawa, A., Kataoko, I., and Michiyoshi, I. (1975), Turbulence Structure of Air–Water Bubbly Flow—I. Measuring Techniques, *Int. J. Multiphase Flow*, **2**, 221.

Wang, M., Mann, R., and Dickin, F. J. (1999), Electrical Resistance Tomographic Sensing Systems for Industrial Applications, *Chem. Eng. Comm.*, **175**, 49.

Wang, M., Jones, T. F., and Williams, R. A. (2003), Visualization of Asymmetric Solids Distribution in Horizontal Swirling Flows Using Electrical Resistance Tomography, *Trans. IChemE.*, **81**, 854.

Wang, M., Ma, Y., Holliday, N., Dai, Y., Williams, R. A., and Lucas, G. P. (2005), A High-Performance EIT System, *IEEE Sens. J.*, **5**, 289.

Wu, Y., Li, H., Wang, M., and Williams, R. A. (2005), Characterization of Air–Water Two-Phase Vertical Flow by Using Electrical Resistance Imaging, *Can. J. Chem. Eng.*, **83**, 37.

Zuber, N. and Findlay, J. A. (1965), Average Volumetric Concentration in Two-Phase Flow Systems, *J. Heat Tran., Trans. ASME,* **87**, 453.